Revista Argentina de Microbiología 55 (2023) 307–316

REVISTA ARGENTINA DE

www.elsevier.es/ram

ORIGINAL ARTICLE

Mycosynthesis of silver nanoparticles using psychrotrophic strains of *Tulasnella albida* Bourdot & Galzin from the South Orkney Islands (Antarctica)

Jesica M. Kobashigawa[a,b], **Carolina A. Robles**[a,b], **Rocío F. Gaiser**[a], **Daniel C. Schinca**[c,d], **Lucía B. Scaffardi**[c,*], **Cecilia C. Carmarán**[a,b,*]

[a] *University of Buenos Aires, Faculty of Exact and Natural Sciences, DBBE Buenos Aires, Argentina*
[b] *CONICET, Institute of Mycology and Botany (INMIBO), Buenos Aires, Argentina*
[c] *Optical Research Center (CIOp) (CONICET - CIC - UNLP), Gonnet, La Plata, Argentina*
[d] *National University of La Plata, Faculty of Engineering, La Plata, Buenos Aires, Argentina*

Received 17 August 2022; accepted 27 April 2023
Available online 19 June 2023

KEYWORDS
Ag nanoparticles;
Antarctic fungi;
Nanotechnology;
Psychrotrophic

Abstract This study is the first report on mycosynthesis of silver nanoparticles (NPs) using psychrotrophic Antarctic filamentous fungi, and the first report regarding *Tulasnella* (Basidiomycota). In this work, the ability to synthesize silver NPs from cell free filtrates of strains of *Tulasnella albida* isolated from Antarctica was assessed. All fungal filtrates were capable of synthesizing silver NPs with the addition of $AgNO_3$. UV–vis spectroscopy, TEM and SEM microscopy analyses were performed to characterize the synthesized NPs. ATR-FTIR and Micro Raman spectroscopy analyses were conducted to find functional groups responsible for the reduction of $AgNO_3$ and to detect the presence of silver oxide on the AgNPs. Theoretical calculations of optical absorption based on core-shell Ag–Ag_2O were used to characterize the experimental absorption spectra of silver NPs colloids. Spherically shaped silver NPs, typically 2–3 nm in diameter, were obtained. The largest ones showed a capping shell around them, which could be associated with the formation of small silver NPs. Functional groups corresponding to amides and alcohols were detected, confirming the presence of proteins as possible intermediates in the synthesis of AgNPs. On the other hand, the Micro Raman analysis confirms the presence of silver oxide on the surface of the AgNPs. This work presents a simple procedure for the synthesis of silver NPs using a psychrotrophic organism that could be interesting for the industry.

* Corresponding authors.
E-mail addresses: lucias@ciop.unlp.edu.ar (L.B. Scaffardi), carmaran@bg.fcen.uba.ar (C.C. Carmarán).

https://doi.org/10.1016/j.ram.2023.04.004

PALABRAS CLAVE
Nanopartículas de plata;
Hongos antárticos;
Nanotecnología;
Psicrotrófico

Micosíntesis de nanopartículas de plata utilizando cepas psicrotróficas de *Tulasnella albida* Bourdot & Galzin de las Islas Orcadas del Sur (Antártida)

Resumen Este estudio constituye el primer informe de micosíntesis de nanopartículas (NP) de plata utilizando hongos filamentosos antárticos psicrotróficos y el primero respecto de *Tulasnella* (Basidiomycota). Se evaluó la capacidad de sintetizar NP de plata a partir de filtrados libres de células de cepas de *Tulasnella albida* aisladas en la Antártida. Todos los filtrados fúngicos fueron capaces de sintetizar NP de plata (AgNP) con la adición de $AgNO_3$. Se realizaron análisis de espectroscopía UV-Vis y microscopía SEM y TEM para caracterizar las NP sintetizadas. Se llevó a cabo un análisis de ATR-FTIR para detectar los posibles grupos funcionales responsables de la reducción del $AgNO_3$ y Micro Raman para identificar la presencia de óxidos de plata recubriendo las AgNP. Se utilizaron cálculos teóricos de absorción óptica basados en NP de Ag-Ag_2O de núcleo-corteza para caracterizar los espectros de absorción experimentales de coloides de AgNP. Se obtuvieron AgNP de forma esférica, típicamente de 2-3 nm de diámetro. Las más grandes mostraban una cubierta protectora a su alrededor, que podría estar asociada con la formación de pequeñas AgNP. Se detectaron grupos funcionales correspondientes a amidas y alcoholes, lo que confirma la presencia de proteínas como posibles intermediarios en la síntesis de AgNP. Por otro lado, el análisis de Micro Raman confirmó la presencia de óxido de plata en la superficie de las AgNP. Este trabajo presenta un procedimiento sencillo para la síntesis de AgNP utilizando un organismo psicrotrófico, que podría ser de interés para la industria.

Introduction

Silver NPs (AgNPs) have a wide range of applications as anti-bacterial agents in the health industry, food storage, textile coatings and several environmental applications as well as electronics and photocatalysis[7]. The synthesis of these nanomaterials through ecological, effective and low-cost methods has become relevant in recent years[34]. Among the organisms used in the green synthesis of AgNPs, fungi are an interesting alternative due to their easy handling and manipulation, tolerance to metals, bioaccumulation capacity and the ability to secrete a wide variety of enzymes[19]. The synthesis of nanomaterials mediated by these organisms has been associated with the presence of fungal enzymes[29].

Extremophile microorganisms are those that are able to grow and thrive in extreme environments, e.g. acidic or alkaline pH, high or low temperatures, high concentrations of pollutants, and salts, among others. Due to their unique physiological and enzymatic characteristics, which allow them to survive in hazardous environments, these organisms are promising for biotechnology[16]. Among extremophiles, psychrophilic organisms have an optimum growth temperature of about 15 °C or less, and cannot grow above 20 °C. On the other hand, psychrotrophic microbes have an optimum growth temperature of 20–30 °C, but are able to grow and exhibit activity at temperatures close to the freezing point of water[11]. The particular characteristics of the metabolism of all these organisms represent valuable assets for advanced industrial applications[28]. In the synthesis of NPs, extremophiles can have a more pronounced ability to withstand conditions that may occur during the industrialization process as well after the act of synthesis, thus adding more stability to the product with specific capping proteins[4]. The ability of the organisms and their proteins to survive in varied conditions also allows for some flexibility in the industrial environment; since the organisms would survive and continue to produce NPs outside optimal conditions, albeit with a lower yield[4].

Antarctica is the largest poorly explored region on Earth and, in a similar way, its mycobiota remains mostly unknown, presenting incalculable value as a scientific preserve and biotechnological repository. Some fungal organisms can grow under the extreme conditions present in the white continent, facing the low temperatures that limit the available water and showing different morphological and physiological adaptive strategies[33]. Among the fungi inhabiting Antarctica, the genus *Tulasnella* J. Schröt, which comprises saprotrophic and mycorrhizal species[27], has been recently registered on decomposing wood from different constructions and artifacts from Deception Island[18] and buildings considered to be historical heritage, such as Casa Moneta Museum, located on the South Orkney Islands[13]. There are few reports about the enzymatic profiles of members of this genus. However, Adamo et al.[1] showed that *Tulasnella calospora* (Boud.) Juel has a robust apparatus for the degradation of crystalline cellulose. We carried out the present study with the aim of studying the potential of Antarctic filamentous fungi in the synthesis of metal NPs. The aims were: (1) to explore the capacity of Antarctic psychrotrophic strains of *Tulasnella albida* Bourdot & Galzin to reduce Ag^+ ions into AgNPs at different temperatures, by comparing their performance and characterize the AgNPs obtained; (2) to assess if there could be a relationship between the production of oxidases, tyrosinases and peroxidases by Antarctic strains of *T. albida*, and the synthesis of NPs.

Material and methods

Chemical compounds

Silver nitrate ($AgNO_3$, Sigma Aldrich) 100 mM was used for the biosynthesis of AgNPs. NaOH (1 M) was used to adjust pH.

Microorganisms

Four psychrotrophic strains of *Tulasnella albida* (BAFCcult 4710, 4711, 4712 and 4713, hereafter referred to as strain 1, strain 2, strain 3 and strain 4, respectively) were used in all the assays. All the strains had been isolated from different wood chips collected, in all cases, from the deteriorated exterior wall of the Casa Moneta Museum located in the South Orkney archipelago, Antarctica, and identified by Gaiser et al.[13]. The exterior wall of the Museum has a double layer of gymnosperm wood with sawdust filling in the middle and is the target of the strongest winds. For detailed sampling methodology please see Gaiser et al.[13]. Orkney station has an annual mean temperature of −4.1 °C varying from 0.9 °C in summer to −11 °C in winter[45]. The strains were grown in 2% malt extract agar (MEA) plates, at 24 °C, and deposited in the culture collection of the Faculty of Exact and Natural Sciences, University of Buenos Aires (BAFCcult).

Growth curve of *Tulasnella albida*

A total of 15 Erlenmeyer flasks containing 50 ml of growth medium were used to evaluate the growth curve of each strain. Growth medium was composed of 10 g l^{-1} glucose, 5 g l^{-1} potato peptone, 3 g l^{-1} malt extract and 3 g l^{-1} yeast extract. The medium was sterilized, inoculated with two 5-mm plugs of each strain, and incubated at 200 rpm at 28 °C, in the dark (modified from Kobashigawa et al.[22]). The fungal biomass from 3 Erlenmeyer flasks (replicates) was harvested every 2 days until day 10, filtered through a filter paper using a Büchner funnel and dried overnight at 40 °C. Then, the dry weight of mycelia was determined. Mean and standard deviation were calculated.

Biosynthesis of AgNPs

For the biosynthesis of AgNPs, the fungal biomass was obtained under the same conditions as for the growth curve, but the incubation lasted 7 days. The fungal biomass obtained was filtered, washed with sterile water and reincubated in 50 ml of sterile distilled water for 3 days, at 200 rpm at 28 °C, in the dark. After the 3 days, the mycelium was filtered, discarding the biomass, and keeping the filtered liquid (hereafter, fungal filtrate). $AgNO_3$ 100 mM was added to the fungal filtrate (0.5 mM final concentration). The fungal filtrate was incubated for 7 days under the same conditions[22]. Both pH 5 and pH 9 were evaluated, by adding NaOH 1 M. Aliquots containing only the fungal filtrate, without salt, and Erlenmeyer flasks containing sterile distilled water with salt were established as controls. After the incubation period, a 1-ml aliquot was removed from each flask to detect the biosynthesis of AgNPs, and their UV–vis spectra were obtained using a spectrophotometer Shimadzu UV-MINI 1240 (Tokyo, Japan) by scanning the absorbance spectra in 200–800 nm range of wavelength. The synthesis of AgNPs was detected by surface plasmon resonance (SPR)[39]. This resonance is due to their small size, but can be influenced by numerous factors that contribute to the exact frequency and intensity of the band. SPR peak of spherical AgNPs is conventionally observed at 400 nm, shifting the position of the plasmon peak to higher wavelengths as the particle radius increases[39]. Only data obtained at pH 9 is informed, as pH 5 treatment gave no positive results.

Given that as-obtained colloid samples may have different NPs size coexisting together, AgNPs synthesized by one of the strains analyzed (selected by showing the best performance in the synthesis) were centrifuged at 15 000 rpm for 20 min as a first step to separate size components. The absorption spectrum of the supernatant was analyzed. As a second step, the supernatant previously obtained was recentrifuged and a new absorption spectrum was recorded[32]. Additionally, NPs obtained were also placed in Falcon tubes, covered, and conserved in a refrigerator for one year. The color and SPR were evaluated.

Modeling

Optical absorption spectra of colloid samples obtained displaying SPR were modeled using the Mie theory for small spherical NPs[5,36]. When Ag^0 atoms (generated by the reduction of Ag^+ ions) nucleate to form the metal core, the oxygen atoms present in the aqueous surrounding medium have a probability to link to the Ag^0 atoms in the surface of the core to form a thin Ag_2O shell, yielding a final core-shell[8] Ag–Ag_2O structure. There is also a biological capping surrounding this nanostructure but, from an optical point of view, it has a refractive index value very similar to water and does not contribute to plasmon peak shifts with respect to pure water. Instead, a thin Ag_2O shell has a sufficiently large refractive index that could be responsible for a possible shift. Taking these facts into account, the Rayleigh approximation for small NPs can be used to determine the polarizability of a core-shell Ag–Ag_2O[7] particle with inner radius r_1, core dielectric function ε_1, outer radius r_2, shell dielectric function ε_2 and surrounding media ε_m:

$$\alpha = 4\pi r_2^3 \frac{(\varepsilon_2 - \varepsilon_m)(\varepsilon_1 + 2\varepsilon_2) + f(\varepsilon_1 - \varepsilon_2)(\varepsilon_m - 2\varepsilon_2)}{(\varepsilon_2 + 2\varepsilon_m)(\varepsilon_1 + 2\varepsilon_2) + f(2\varepsilon_2 - \varepsilon_m)(\varepsilon_1 - \varepsilon_2)}$$

where $f = (r_1/r_2)^3$. Metallic dielectric function was obtained from Johnson and Christy[21] while shell dielectric function was taken from Qiu et al.[30].

AgNPs synthesis efficiency

To study the formation of AgNPs for each strain, absorption spectra were taken on days 1, 2, 3 and 7 after the beginning of incubation. Efficiency was defined as the height of the SPR when the maximum absorbance peak of the SPR band was measured in each spectrum for the stated days[22], always under the same conditions of time, temperature and concentration. Five replicates of the synthesis were performed. Mean and standard deviation were calculated.

Study of NPs synthesis at low temperature

The capability of synthesis of AgNPs of strain 2 was tested using the same procedure as the biosynthesis at 28 °C. The strain was grown at 6 °C to produce biomass and the biosynthesis of AgNPs was also carried out at 6 °C. Absorbance was measured until day 3. Additionally, a new measure was performed on these NPs kept at 6 °C for 2 years. Five replicates were performed. Mean and standard deviation of dry weight of the mycelium was calculated.

Characterization of AgNPs and fungal filtrates

AgNPs were characterized using a scanning electron microscope (SEM) model Zeiss SUPRA TM 40 (Oberkochen, Germany) in the secondary electron mode, and with a FEI-Talos F200X G2 FEG scanning transmission electron microscope in STEM mode combined with a high angle annular dark field (HAADF) detector, 0.16 nm of resolution. Energy-dispersive X-ray spectroscopy (EDS) was conducted on the sample. Micro Raman spectroscopy was conducted for detecting the presence of silver oxide on dried samples using a confocal HORIBA ExPlora Plus Raman Microscope, working with an excitation wavelength of 785 nm. Functional groups responsible for the reduction of $AgNO_3$ and capping of synthesized AgNPs were detected using attenuated total reflectance in conjunction with FTIR spectrophotometer (ATR-FTIR) ranging from 400 to 4000 cm^{-1} (Thermo Scientific Nicolet iS50) over a freeze-dried sample of NPs. Additionally, analyses were performed on the fungal filtrate to detect total protein by the Bradford method[6] with bovine serum albumin as the standard, and reducing sugars by the Somogyi–Nelson procedure[25] with glucose as a standard. Considering the similarities between the SPR obtained for the four strains, AgNPs characterizations were conducted only on strain 2.

Enzymatic reactions

Oxidase reactions were performed using gallic and tannic acid media and tyrosine Agarized media was used to detect the presence of tyrosinase[42]. For the detection of lignin peroxidase activity (LiP), reactions were assayed in culture media with Azure B. Additionally, a decolorization test of malachite green was performed to detect the activity of the manganese peroxidase[23]. The assays were performed in Petri dishes and the reactions were considered positive when a color change was observed in the corresponding culture medium after one-week incubation in the dark at 24 °C. The relative intensity of the reaction (+/−) was recorded. All reactions were performed twice.

Results

Growth curve of *Tulasnella albida*

A growth curve of dry weight as a function of time was made for the four strains (Supplementary Figure S1). All strains showed an initial lag growth phase between days 2 and 4, and then an exponential growth phase. In the case of strain 1 and strain 2, the deceleration phase seems to have started on day 8.

Biosynthesis of AgNPs

As a result of the biosynthesis assay, spectra of all strains showed the typical Ag plasmon resonance in the range 400 and 430 nm on day 7. A second maximum was observed at about 210 nm, along with a smaller absorption band in the 230–300 nm range (Fig. 1A). Figure 1B shows the three spectra of the centrifuged colloids from strain 2. Figure 1B also shows a calculated optical extinction spectrum of a core-shell NPs using the Mie theory. For this case, a core radius $r_1 = 0.9$ nm and an outer radius $r_2 = 1.05$ nm were used. Experimental SPR peak position of the supernatant redispersed colloid was reproduced. For the four strains, absorbance at 420 nm at the time of synthesis/and after one year were obtained: strain 1: 2.95/3.91; strain 2: 3.1/3.87; strain 3: 3.25/3.93; strain 4: 3.02/3.44.

AgNPs synthesis efficiency

The gradually progressing reaction of AgNPs synthesis was monitored using UV–vis spectrometry (since the intensity of the plasmon peak is proportional to the concentration of AgNPs produced) (Fig. 1C). All the spectra exhibited an intense peak corresponding to the SPR of AgNPs, implying the bioreduction of $AgNO_3$ in the fungal filtrate. Strain 2 presented a higher absorbance than the other strains, suggesting a higher production of AgNPs.

Study of NPs synthesis at low temperature

The assay performed showed that strain 2 can grow at low temperatures producing a biomass of 32.6 ± 6.7 mg after 7 days. With regard to the biosynthesis assays, Figure 1D shows the absorbance of the synthesis product at 6 °C on day 3. Compared to the absorbance of the NPs synthesized at 28 °C (day 3), the plasmon height was around 4.4 times lower (3.071 absorbance at 28 °C; 0.706 absorbance at 6 °C), a similar relationship was obtained with biomass data, with a relationship of around 4.8 (0.1557 g at 28 °C/0.0326 g at 6 °C).

A colored colloid of AgNPs (6 °C) (inset of Fig. 1D) was obtained showing a lighter color compared with the AgNPs (28 °C) (inset of Fig. 1A). In Figure 1D, a theoretical calculation of the absorption spectrum for a core-shell – NPs with 0.4 nm inner radius and 0.46 outer radius is shown. This spectrum shows a good agreement with the experimental plasmon resonance of AgNPs synthesized at 6 °C.

The analysis of the absorption spectra of the colloid obtained 2 years later shows the presence of the plasmon with a slightly weaker signal. Moreover, the color of the sample became lighter.

Characterization of AgNPs and fungal filtrate

Several techniques were used for morphological and compositional NPs characterization. Taking into consideration the similar results of the absorbance spectra, only the NPs

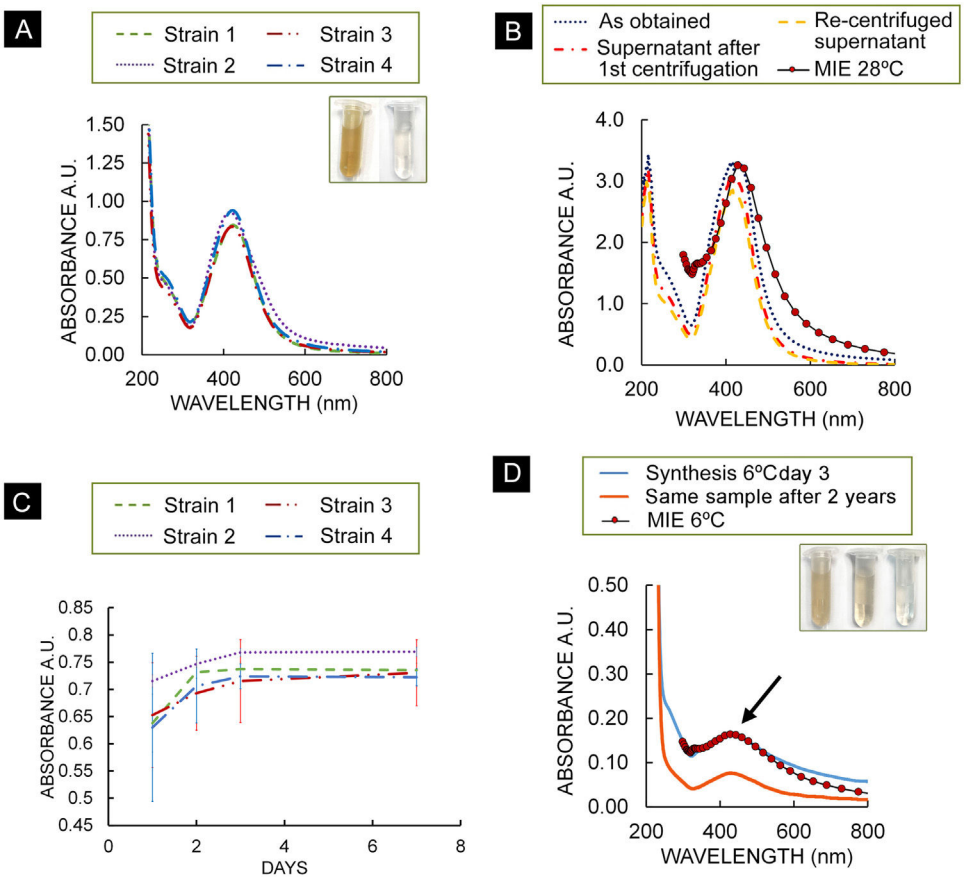

Figure 1 (A) Absorption spectra of strains of *T. albida*, dilution 1:4; inset in (A): colloid of NPs synthesized by strain 2 at 28 °C (left) and fungal filtrate (right). (B) Absorption spectra of the as-obtained colloid (strain 2), supernatant after first centrifugation and recentrifuged supernatant and theoretical calculation of absorption spectra. (C) Maximum absorbance of each *T. albida* strain over time, dilution 1:4. Bars show standard deviation. (D) Absorption spectra of colloid obtained using strain 2 at 6 °C on day 3, theoretical calculation of absorption spectrum for Ag–Ag_2O NPs and absorption spectra of the same sample taken 2 years later, in both cases typical Ag plasmon resonance was observed (arrow); inset in (D): colloid NPs obtained at 6 °C were obtained (left), same sample 2 years later (middle) and fungal filtrate (right).

synthesized at 28 °C were characterized. The SEM images in Figures 2A and B show isolated and aggregated AgNPs. The AgNPs were not in direct contact even within the aggregates,

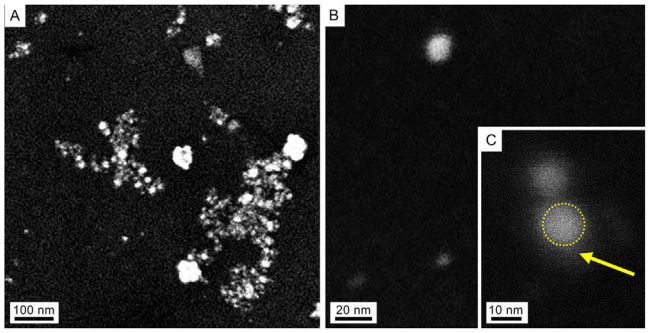

Figure 2 SEM images of colloidal AgNPs synthesized by strain 2 in secondary electron mode (accelerating voltage 3 kV). (A) Panoramic view of AgNPs, showing isolated NPs as well as some agglomerates produced in the drying process of the sample. (B) Isolated NP. (C) Detail of an AgNP (dotted circle) and capping (arrow).

indicating that the capping agent is effective in keeping the AgNPs isolated (Figs. 2B and C).

With regard to the TEM images of synthesized NPs, Figure 3A shows a panoramic view of synthesized NPs where isolated NPs and some agglomerates produced by the drying process are observed. Figure 3B shows a close-up on the 20 nm scale where isolated spherical NPs are observed. A brighter center surrounded by a lighter area is observed in some of the NPs. Panel C is a high-resolution image of typical core-shell NPs, where curved dashed lines indicate the limits of NP and capping. The size histogram corresponding to panel (B) shows a size distribution with a maximum at about 2–3 nm diameter (Fig. 3D).

An elemental composition analysis of a HAADF image of a couple of AgNPs was conducted. Results are shown in Figure 4. Figure 4A shows isolated colloidal AgNPs, surrounded by a whitish cloud. Figure 4B reveals the presence of Ag atoms in green colored dots. It can be observed that they are concentrated in the NPs and their close surroundings (capping). Similar signals are also observed in the background of the image, indicating the presence of small amounts of silver. Elemental oxygen atom distribution over

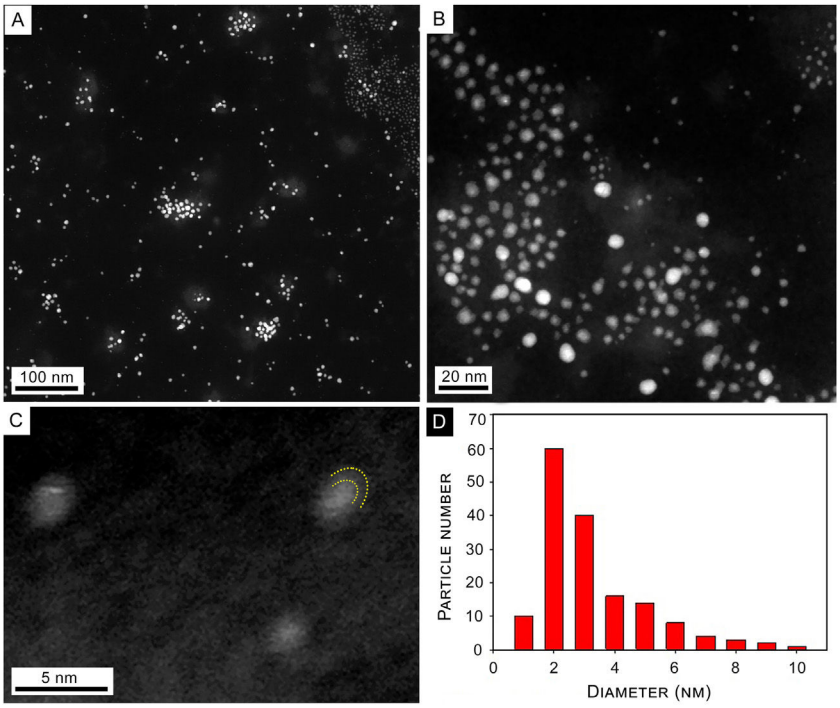

Figure 3 STEM HAADF images of colloidal AgNPs produced by strain 2. (A) Panoramic view. (B) Detail of spherical NPs. (C) High resolution image of typical core-shell NPs. Curved dashed lines show the limits of NP and capping. (D) Size histogram of NPs corresponding to panel (B).

the same area is depicted in Figure 4C, showing a clear concentration on the core-shell NPs, while panel D shows these two elements superimposed.

Figure 4E shows the EDS spectrum for the selected area at the NPs of panel A. The three maxima corresponding to Ag are clearly observed, as well as that of oxygen. Cu and C peaks correspond to the interaction of the electron beam with the sample holder. A similar spectrum for a region away from the NP is shown in Figure 4F, where Ag peaks are observed with negligible intensity. The C and Cu peaks in both panels 4E and 4F arose from the grid. The O peak that appears in both panels may correspond to the oxidation of metals. Small amounts of oxygen and carbon could be attributed to the organic layer forming the capping on the synthesized AgNPs.

Micro Raman spectroscopy was used on different zones of several dried drops of samples placed over a coverglass to help determine the chemical composition of the NPs. A total of 40 spectra between 200 cm^{-1} and 1200 cm^{-1} were taken. Figure 5 shows a typical Raman spectrum. Raman shifts indicated by arrows at 240, 490 and 565 cm^{-1} are generally assigned to bulk Ag_2O stretching vibrations[24]. The bands at about 1070 cm^{-1} are attributed by some authors to chemisorbed oxygen molecules on the NP surface[40,47], although there is general consensus in assigning them to Ag–O bending modes[24]. These bands reveal the presence of Ag_2O bonds in the analyzed samples.

FTIR spectra (Fig. 6) showed peaks at 3278, 2917, 1620, 1333, 1030, 832, 766, 693 and 439 cm^{-1}. The peak at 3278 represents the O–H bonds of alcohols and phenols and the peak at 2917 can be assigned to C–H stretching of alkane compounds[32]. The peaks at 1620, 1550 and 1333 cm^{-1} could be assigned to the amide I, II and III band of proteins[17]. The peak at 1030 could be assigned to C–N stretching vibrations of aliphatic amines[38]. The peak at 766 could be assigned to alkane C–H bending[44].

Negligible values (close to cero) were obtained through the Bradford and Somogyi–Nelson procedure over the fungal filtrate perhaps due to the low presence of these compounds in the filtrate.

Enzymatic reactions

Enzymatic reactions were negative for all media and strains evaluated, except for malachite green that resulted in a halo of mild discoloration in all the strains evaluated (Supplementary Figure S2).

Discussion

This is the first report of mycosynthesis performed to evaluate psychrotrophic Antarctic filamentous fungi, and the first report regarding the genus *Tulasnella*. The data obtained showed that, on day 7, all strains were in the exponential phase of growth and were capable of producing the metabolites necessary for the synthesis of NPs. The four strains evaluated showed the ability to synthesize AgNPs, with strain 2 having the highest efficiency, suggesting that the ability to synthesize AgNPs is strain-dependent. Similar results were obtained by Ganbarov et al.[14] with *Fusarium oxysporum* Schltdl. The characteristic plasmon band around 400–430 nm of synthesized AgNPs, confirmed the presence of these NPs and reached a stable population after 3 days.

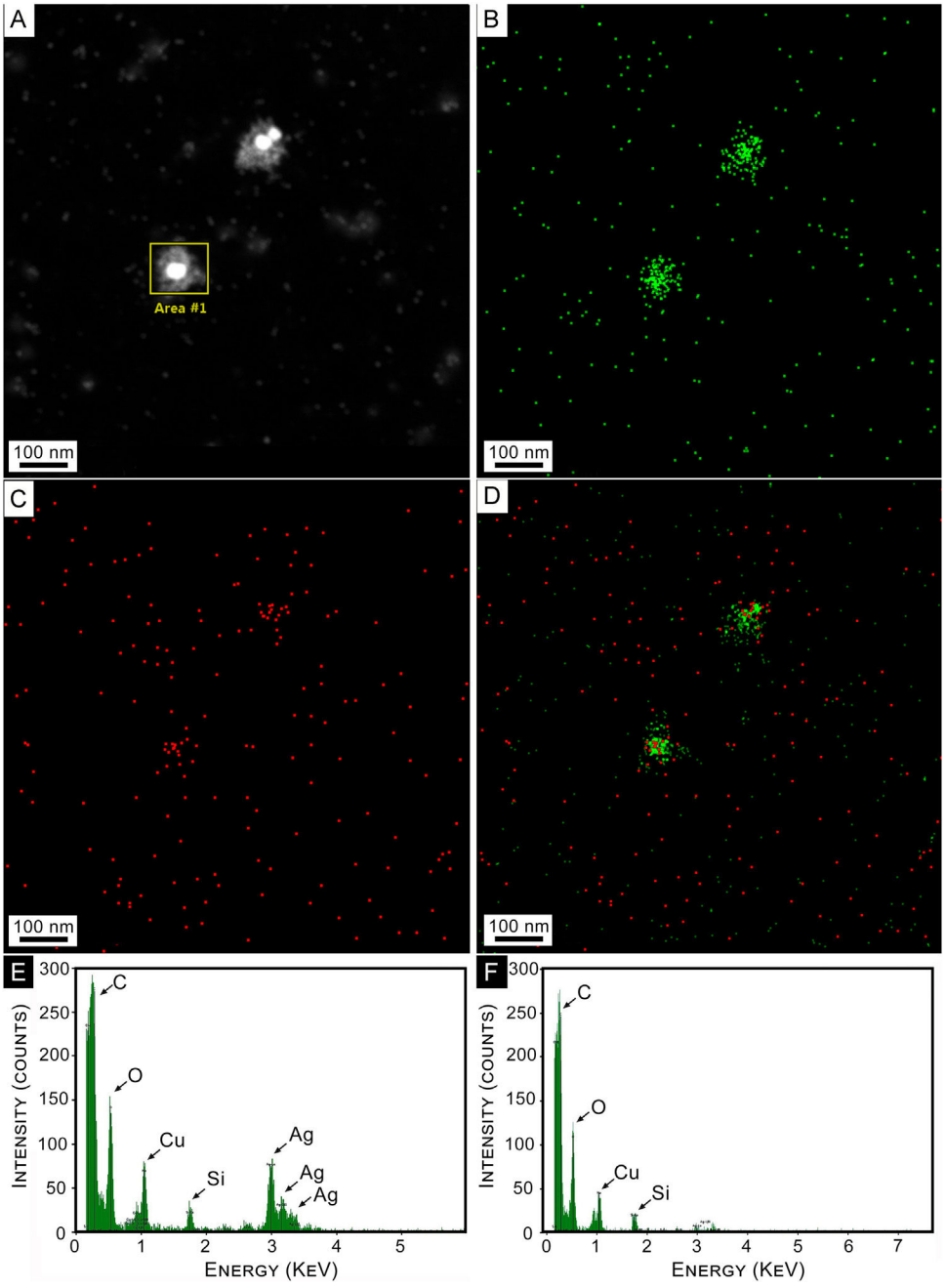

Figure 4 Composition analysis. (A) STEM Dark Field Images (HAADF) of colloidal AgNPs synthesized by strain 2. (B) EDS mapping of HAADF image of panel (A) for Ag. (C) EDS mapping of HAADF image of panel (A) for O. (D) Superimposed mapping of Ag and O. (E) EDS elemental composition for selected area at NP of panel (A). (F) EDS Elemental composition for a region far away from the selected area of panel (A).

Tulasnella albida had the ability to synthesize AgNPs at 6 °C, showing that strains recovered from Antarctica could be used in processes of synthesis at suboptimal conditions. Similar results were obtained by Gemishev et al.[15]. In this work the authors synthesized AgNPs using *Trichoderma reesei* E.G. Simmons at different temperatures, including 4 °C, and suggested that the slow rate of the reaction is due to the low enzyme activity at that temperature. AgNPs synthesized at 28 °C maintained a similar plasmon peak after one year, although AgNPs synthesized at 6 °C showed a decrease in plasmon height after two years, probably because they are less stable.

Several microorganisms have been used in the synthesis of AgNPs; however, just a few reports used psychrotrophic fungi. Among fungi, the yeasts *Papiliotrema laurentii* (Kuff.) Xin Zhan Liu, F.Y. Bai, M. Groenew. & Boekhout[26] and *Yarrowia lipolytica* (Wick., Kurtzman & Herman) Van der Walt & Arx[3] have been evaluated. Fayaz et al.[10] and Ahluwalia et al.[2] registered the synthesis of AgNPs at 10 °C using the filamentous fungi *Trichoderma viride* Pers. grown

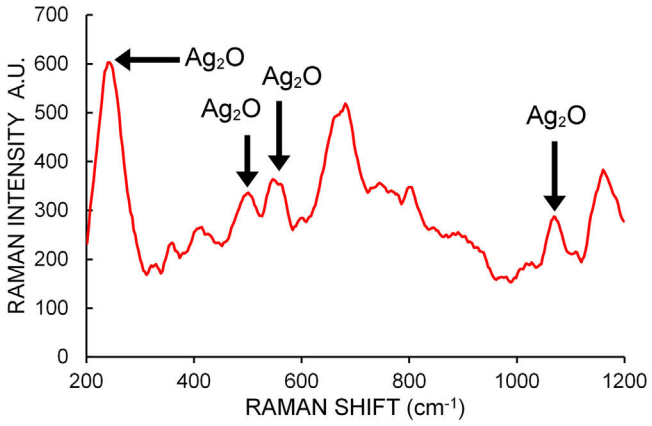

Figure 5 Raman spectrum of a dried drop of AgNPs colloidal suspension synthesized by *T. albida* strain 2. Arrows indicate the characteristic Raman peaks of Ag_2O.

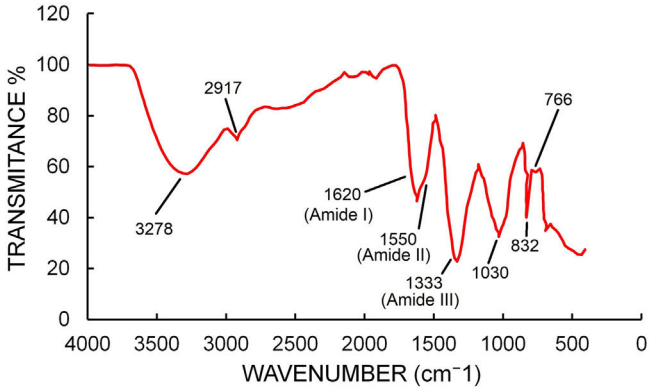

Figure 6 FTIR-ATR spectra of freeze-dried samples of AgNPs synthesized by *T. albida* strain 2.

at 27 °C. The authors reported an increase in size mediated by the temperatures of the synthesis, and the plasmon obtained shifted toward higher wavelengths. In the present study the theoretical model suggests a decrease in NPs size at low temperature of synthesis similar to the results reported by Javani et al.[20].

Concerning the absorption spectra, it is known that biogenic species display absorption bands in the UV due to protein molecules present in the extract, for example as stated by Sharma et al.[37]. In our experiments, this fact was carefully taken into account in the absorbance determination process using as reference the same extract (background) as the one used for NPs synthesis (sample). Under this condition, the absorption band in the range 200–300 nm could be due to the excitation of silver interband transitions and also the presence of few-atoms Ag nanoclusters (proto NPs) suspended in the sample. Santillán et al.[35] reported the same band when studying Ag clusters fabricated in pure water by laser ablation (without biological compounds), indicating the same origin of the band. During the centrifugation steps, the plasmon band decreased in intensity while the UV absorption band remained approximately constant. This could indicate that the number of AgNPs decreases faster than nanoclusters in the centrifugation process.

AgNPs obtained using *T. albida* resulted in a spherical shape of about 2–3 nm, having a capping material surrounding them. The maximum SPR peak reached was on day 3, similarly to wood decay fungi *Trametes trogii*[22]. Although the malachite green test has been positive, ligninolytic enzymes do not seem to be present. The decoloration halo seen in malachite green medium might be attributed to another metabolic pathway such as hydroquinone[41]. Therefore, it could be considered that ligninolytic enzymes are not related to the synthesis of AgNPs in the genus *Tulasnella*. Other authors proposed the role of NADH-dependent nitrate reductase in NPs biosynthesis[31]. Previous reports on *T. calospora* (Boud.) Juel showed that this enzyme is not present in the metabolism of the genus *Tulasnella*[12]. On the other hand, Ehsan et al. while studying the secretome of *T. calospora* reported the presence of a high number of small, secreted proteins that are mainly glycoside hydrolases and thaumatin-like proteins[9]. Additionally, Wanarska and Maliszewska[46] proposed the role of polysaccharides and other polypeptides as mediators of the synthesis of AgNPs. It should be noted that the measurements of total proteins and reducing sugars using the methodology of this work did not show any results due to the low presence of these compounds in the fungal filtrate. This result may be of interest given the great reducing power observed for the synthesis of AgNPs despite the low presence of proteins in the synthesis medium. Detailed studies evaluating the possible mechanism involved in the synthesis of AgNPs are necessary to elucidate the role of components during the process of synthesis. The FTIR-ATR spectra showed that proteins are present, indicating a possible role in the synthesis of AgNPs. On other hand, the images obtained from EDS showed that the area occupied by capping had small clusters of Ag, suggesting that the capping could play a role as a reducing agent. Sytu and Camacho[43], using *Lenzites betulinus* (L.) Fr., suggested that the biological capping of nanoparticles is composed of protein and polypeptide molecules. Functional groups such as carboxyl, hydroxyl, and amide groups of the proteinaceous capping molecules could participate in the reduction and stabilization process of AgNPs. The results of the present study agree with the hypothesis that the reduction of Ag continues at the expense of the capping macromolecules.

The chemical composition of NPs was studied using different techniques. Optical extinction spectra (OES) of the different stains were carried out, taking into account the corresponding biological background. In all of them, plasmon absorbance peaks at about 425 nm were observed, indicating the presence of metallic silver NPs. The absorbance features observed for wavelengths smaller than 300 nm may be assigned to silver interband transitions and to the presence of small clusters (proto NPs), which also support the proposed metallic composition of the nanoparticle. Typical plasmon resonance for small AgNPs in water is centered at 400 nm. The observed shift can be due to three reasons: NP size in excess of 30 nm, environmental refractive index or the presence of a shell around the silver core. From the TEM analysis, the typical NP size in our samples is smaller than 20 nm according to the histogram performed, ruling out the first reason. Since NPs are suspended in an environment mainly composed of water, the second reason cannot be responsible for the observed plasmon shift. Since silver is

prone to oxidation in the presence of an aqueous solution, it is plausible to argue that a silver oxide shell is formed around the silver metal core. The experimental spectra corresponding to colloidal NPs immersed in biological material exhibit the peak position at 425 nm. The excellent fit (shape and plasmon peak location) using the Rayleigh approximation to the Mie theory supports the argument that Ag–Ag_2O structures are present in the colloid. On the contrary, it is worth noting that without considering an Ag_2O shell, the fit would not have been good and the peak would not have been red-shifted up to 425 nm.

On the other hand, the Micro Raman analysis over several zones on dried drop samples showed Raman shifts corresponding to stretching and vibrations of Ag_2O bonds, confirming the presence of this type of oxide. The complementary analysis performed by EDS mapping images over selected NPs, shows the presence of silver and oxygen, indicating that both elements are available for the combination of Ag_2O.

Conclusion

The present work provides evidence that the Antarctic strains of *T. albida* are capable of synthesizing AgNPs with a high performance at 28 °C, and that this biosynthesis process could occur at low temperatures (6 °C). The NPs obtained have spherical shapes with sizes between 1 and 10 nm with a structure of core shell Ag–Ag_2O. Additionally, our findings suggest the presence of nanoclusters of Ag and their locations indicate that the capping acts as a reducing agent. On the other hand, the mechanism of NPs synthesis remains unknown. However, the characterization performed here and the information reported by other authors indicate that neither ligninolytic enzymes nor NADH-dependent nitrate reductase play a relevant role in the synthesis of AgNPs in *T. albida*. Cold-adapted microorganisms have a great potential in biotechnological application, offering numerous advantages: growth capacity, enzymatic activities, and catalytic efficiencies at low temperature range, preventing the risk of microbial contamination and even energy saving. These capabilities grant flexibility in industrialization processes, allowing development outside optimal conditions. Our study presents new findings that contribute to the knowledge of extremophilic organisms and their potential use in nanotechnology.

Conflict of interest

The authors declare that they have no conflict of interest.

Acknowledgement

We acknowledge Dr. A. Caneiro from Y-TEC S.A. Argentina for the use of TEM FEI TALOS F200X, as well as for his commitment and dedication. This study was supported by PIP 0956 and 0280 (CONICET Argentina), MINCyT-PME 2006-00018, 11/I197, Engineering Faculty (UNLP) and UBACyT 20020190100051BA (UBA), pict 2020-00513 and pict 2020-01147 (Anpyct).

Appendix A. Supplementary data

Supplementary data associated with this article can be found, in the online version, at doi:10.1016/j.ram.2023.04.004.

References

1. Adamo M, Chialva M, Calevo J, De Rose S, Girlanda M, Perotto S, Balestrini R. The dark side of orchid symbiosis: can *Tulasnella calospora* decompose host tissues? Int J Mol Sci. 2020;21:3139.
2. Ahluwalia V, Kumar J, Sisodia R, Shakil NA, Walia S. Green synthesis of silver nanoparticles by *Trichoderma harzianum* and their bio-efficacy evaluation against *Staphylococcus aureus* and *Klebsiella pneumonia*. Ind Crops Prod. 2014;55:202–6.
3. Apte M, Sambre D, Gaikawad S, Joshi S, Bankar A, Kumar AR, Zinjarde S. Psychrotrophic yeast *Yarrowia lipolytica* NCYC 789 mediates the synthesis of antimicrobial silver NPs via cell-associated melanin. AMB Express. 2013;3:1–8.
4. Beeler E, Singh OV. Extremophiles as sources of inorganic bionanoparticles. World J Microbiol Biotechnol. 2016;32:1–11.
5. Bohren CF, Huffman DR. Absorption and scattering of light by small particles. New York: John Wiley and Sons, Inc.; 1998. p. 130–6.
6. Bradford MM. A rapid and sensitive method for the quantitation of microgram quantities of protein utilizing the principle of protein-dye binding. Anal Biochem. 1976;72:248–54.
7. Calderón-Jiménez B, Johnson ME, Montoro Bustos AR, Murphy KE, Winchester MR, Vega Baudrit JR. Silver nanoparticles: technological advances, societal impacts, and metrological challenges. Front Chem. 2017;5:6.
8. Chatterjee K, Sarkar S, Rao KJ, Paria S. Core/shell nanoparticles in biomedical applications. Adv Colloid Interface Sci. 2014;209:8–39.
9. Ehsan T, Reza RN, Das A, Ahmed O, Baten AA, Ferdous AS, Islam MR, Khan H. Genome and secretome analysis of jute endophyte *Grammothele lineata* strain SDL-CO-2015-1: insights into its lignocellulolytic structure and secondary metabolite profile. Genomics. 2020;112:2794–803.
10. Fayaz AM, Balaji K, Kalaichelvan PT, Venkatesan R. Fungal based synthesis of silver nanoparticles – an effect of temperature on the size of particles. Colloids Surf B Biointerfaces. 2009;74:123–6.
11. Fendrihan S, Negoita TG. Psychrophilic microorganisms as important source for biotechnological processes. In: Stan-Lotter H, Fendrihan S, editors. Adaption of microbial life to environmental extremes. Springer: Cham; 2017. p. 147–99.
12. Fochi V, Chitarra W, Kohler A, Voyron S, Singan VR, Lindquist EA, Barry KW, Girlanda M, Grigoriev IV, Martin F, Balestrini R, Perotto S. Fungal and plant gene expression in the *Tulasnella calospora–Serapias vomeracea* symbiosis provides clues about nitrogen pathways in orchid mycorrhizas. New Phytol. 2017;213:365–79.
13. Gaiser RF, Robles CA, Kobashigawa JM, Pereira S, Skronski N, Carmarán CC. Mycobiota associated to Casa Moneta Museum wood, South Orkney Islands, Antarctica. Polar Biol. 2021;44:1817–31.
14. Ganbarov KG, Ahmadov IS, Ramazanov MA, Musayev EM, Eyvazova QI, Aghamaliyev ZA. Silver nanoparticles synthesized by the Azerbaijanian environmental isolates *Aspergillus niger*. J Microbiol Biotechnol Food Sci. 2014;4:137–41.
15. Gemishev O, Panayotova M, Gicheva G, Mintcheva N. Green synthesis of stable spherical monodisperse silver nanoparticles using a cell-free extract of *Trichoderma reesei*. Materials. 2022;15:481.

16. Giovanella P, Vieira GA, Otero IVR, Pellizzer EP, de Jesus Fontes B, Sette LD. Metal and organic pollutants bioremediation by extremophile microorganisms. J Hazard Mater. 2020;382:121024.
17. Glassford SE, Byrne B, Kazarian SG. Recent applications of ATR FTIR spectroscopy and imaging to proteins. Biochim Biophys Acta. 2013;1834:2849–58.
18. Held BW, Blanchette RA. Deception Island, Antarctica, harbors a diverse assemblage of wood decay fungi. Fungal Biol. 2017;121:145–57.
19. Hulkoti NI, Taranath TC. Biosynthesis of nanoparticles using microbes – a review. Colloids Surf B Biointerfaces. 2014;121:474–83.
20. Javani S, Marín I, Amils R, Abad JP. Four psychrophilic bacteria from Antarctica extracellularly biosynthesize at low temperature highly stable silver nanoparticles with outstanding antimicrobial activity. Colloids Surf A Physicochem Eng Asp. 2015;483:60–9.
21. Johnson PB, Christy RW. Optical constants of the noble metals. Phys Rev B. 1972;6:4370.
22. Kobashigawa JM, Robles CA, Martínez Ricci ML, Carmáran CC. Influence of strong bases on the synthesis of silver nanoparticles (AgNPs) using the ligninolytic fungi *Trametes trogii*. Saudi J Biol Sci. 2019;26:1331–7.
23. Levin L, Forchiassin F, Viale A. Ligninolytic enzyme production and dye decolorization by *Trametes trogii*: application of the Plackett–Burman experimental design to evaluate nutritional requirements. Process Biochem. 2005;40:1381–7.
24. Martina I, Wiesinger R, Jembrih-Simbürger D, Schreiner M. Micro-Raman characterisation of silver corrosion products: instrumental set up and reference database. e-Preserv Sci. 2012;9:1–8.
25. Nelson N. A photometric adaptation of the SOMOGYI method for the determination of glucose. J Biol Biochem. 1944;153:375–80.
26. Ortega FG, Fernández-Baldo MA, Fernández JG, Serrano MJ, Sanz MI, Diaz-Mochón JJ, Lorente JA, Raba J. Study of antitumor activity in breast cell lines using silver nanoparticles produced by yeast. Int J Nanomed. 2015;10:2021.
27. Preußing M, Nebel M, Oberwinkler F, Weiß M. Diverging diversity patterns in the *Tulasnella* (Basidiomycota, Tulasnellales) mycobionts of *Aneura pinguis* (Marchantiophyta, Metzgeriales) from Europe and Ecuador. Mycorrhiza. 2010;20:147–59.
28. Purcarea C, Necula-Petrareanu G, Vasilescu A. Extremophile-assisted nanomaterial production and nanomaterial-based biosensing. In: Dinca V, Suchea MP, editors. Functional nanostructured interfaces for environmental and biomedical applications. Elsevier; 2019. p. 153–80.
29. Qamar SUR, Ahmad JN. Nanoparticles: mechanism of biosynthesis using plant extracts, bacteria, fungi, and their applications. J Mol Liq. 2021;334:116040.
30. Qiu JH, Zhou P, Gao XY, Yu JN, Wang SY, Li J, Chen LY. Ellipsometric study of the optical properties of silver oxide prepared by reactive magnetron sputtering. J Korean Phys Soc. 2005;46:269.
31. Rai M, Bonde S, Golinska P, Trzcińska-Wencel J, Gade A, Abd-Elsalam K, Ingle A. *Fusarium* as a novel fungus for the synthesis of nanoparticles: mechanism and applications. J Fungi (Basel). 2021;7:139.
32. Rani R, Sharma D, Chaturvedi M, Yadav JP. Green synthesis, characterization and antibacterial activity of silver nanoparticles of endophytic fungi *Aspergillus terreus*. J Nanomed Nanotechnol. 2017;8:457.
33. Ruisi S, Barreca D, Selbmann L, Zucconi L, Onofri S. Fungi in Antarctica. Rev Environ Sci Biotechnol. 2007;6:127–41.
34. Salem SS, Fouda A. Green synthesis of metallic nanoparticles and their prospective biotechnological applications: an overview. Biol Trace Elem Res. 2021;199:344–70.
35. Santillán JMJ, Muñetón Arboleda D, Muraca D, Schinca DC, Scaffardi LB. Highly fluorescent few atoms silver nanoclusters with strong photocatalytic activity synthesized by ultrashort light pulses. Sci Rep. 2020;10:1–13.
36. Schinca DC, Scaffardi LB. Core and shell sizing of small silver-coated nanospheres by optical extinction spectroscopy. Nanotechnology. 2008;19:495712.
37. Sharma G, Nam JS, Sharma AR, Lee SS. Antimicrobial potential of silver nanoparticles synthesized using medicinal herb coptidis rhizome. Molecules. 2018;23:2268.
38. Singh D, Rathod V, Ninganagouda S, Hiremath J, Singh AK, Mathew J. Optimization and characterization of silver nanoparticles by endophytic fungi *Penicillium* sp. isolated from *Curcuma longa* (turmeric) and application studies against MDR *E. coli* and *S. aureus*. Bioinorg Chem Appl. 2014;2014:408021.
39. Slistan-Grijalva A, Herrera-Urbina R, Rivas-Silva JF, Ávalos-Borja M, Castillón-Barraza FF, Posada-Amarillas A. Classical theoretical characterization of the surface plasmon absorption band for silver spherical nanoparticles suspended in water and ethylene glycol. Physica E Low Dimens Syst Nanostruct. 2005;27:104–12.
40. Socrates G. Infrared and Raman characteristic group frequencies: tables and charts. Chichester: John Wiley and Sons; 2001.
41. Song J, Han G, Wang Y, Jiang X, Zhao D, Li M, Yang Z, Ma Q, Parales R, Ruan Z, Mu Y. Pathway and kinetics of malachite green biodegradation by *Pseudomonas veronii*. Sci Rep. 2020;10:4502.
42. Stalpers JA. Identification of wood-inhabiting fungi in pure culture. Stud Mycol. 1978;16:1–248.
43. Sytu MRC, Camacho DH. Green synthesis of silver nanoparticles (AgNPs) from *Lenzites betulina* and the potential synergistic effect of AgNP and capping biomolecules in enhancing antioxidant activity. BioNanoScience. 2018;8:835–44.
44. Thakor R, Mistry H, Patel H, Jhala D, Parmar N, Bariya H. Biogenic synthesis of silver nanoparticles mediated by the consortium comprising the marine fungal filtrates of *Penicillium oxalicum* and *Fusarium hainanense* along with their antimicrobial, antioxidant, larvicidal and anticancer potency. J Appl Microbiol. 2022;133:857–69, http://dx.doi.org/10.1111/jam.15611.
45. TuTiempo.net. Clima en BASE ORCADAS. https://www.tutiempo.net/clima/2019/ws-889680.html [accessed 09.07.22].
46. Wanarska E, Maliszewska I. The possible mechanism of the formation of silver nanoparticles by *Penicillium cyclopium*. Bioorg Chem. 2019;93:102803.
47. Wang C-B, Deo G, Wachs IE. Interaction of polycrystalline silver with oxygen, water, carbon dioxide, ethylene, and methanol: in situ Raman and catalytic studies. J Phys Chem B. 1999;103:5645–56.